ELSEVIER

Contents lists available at ScienceDirect

Additive Manufacturing

journal homepage: www.elsevier.com/locate/addma





Modeling of two-photon polymerization in the strong-pulse regime

Mingman Sun^{a,1}, He Cheng^b, Pooria Golvari^c, Stephen M. Kuebler^{b,c,d}, Xiaoming Yu^b, Meng Zhang^{a,*}

- ^a Department of Industrial and Manufacturing Systems Engineering, Kansas State University, Manhattan, KS 66506, USA
- ^b CREOL, The College of Optics and Photonics, University of Central Florida, Orlando, FL 32816, USA
- ^c Department of Chemistry, University of Central Florida, Orlando, FL 32816, USA
- ^d Department of Materials Science and Engineering, University of Central Florida, Orlando, FL 32816, USA

ARTICLE INFO

Keywords: Additive manufacturing Bessel beam Femtosecond laser Model Two-photon polymerization

ABSTRACT

This paper reports a study of two-photon polymerization induced by femtosecond laser pulses having microjoule pulse energy and kilohertz repetition rates. Light-matter interaction and polymerization kinetics are modeled in highly confined spatiotemporal scales. The model employs a non-diffractive Bessel beam, considers the effects of temperature-dependent species diffusions, and regards propagation and termination kinetic constants as functions of double-bond conversion. The model is validated by comparing the size of features predicted from simulations to those generated experimentally. The model is used to investigate how the time and energy required to create a single volume element ("voxel") change under various conditions of irradiation. The results show that polymerizing a single voxel requires a minimum exposure time that is constant across a range of irradiation conditions, and is largely determined by the chemical kinetics. In the regime where the pulse energy is low (< 10 μ J), it is more energy-efficient to use fewer pulses having higher energy within the same total exposure time. However, this trend reverses in the regime where the pulse energy is high (10μ J - 30μ J), because radical-radical recombination becomes significant, which wastes absorbed energy. This work advances the understanding of two-photon polymerization in the strong-pulse regime and is a step toward increasing throughput to a level suitable for industrial applications.

1. Introduction

Most additive manufacturing (AM) technologies involve joining materials together layer by layer to fabricate an object according to a 3D model [1,2]. This layer-by-layer fashion inherently limits AM's potentials in surface quality, repeatability, and fabrication throughput [3,4]. Volumetric AM based on two-photon polymerization (TPP) uses femtosecond laser pulses to produce a highly localized photopolymerization reaction inside a resin volume and fabricate microscale structures with unrivaled 100–200 nm resolution [5–8]. TPP differs in several significant ways from one-photon methods, such as stereolithography (SLA) [9] and digital light processing (DLP) [10]. With TPP, the active zone is confined to a small volume around the geometric focal point and is localized by the combined effects of optical and chemical nonlinearity. Simultaneous absorption of two photons by a photoinitiator activates a chemical reaction that can form active species like free radicals. The initiating radical can react with the monomer forming

a new bond along with another radical that resides on the monomer itself. The monomer-centered radical can then react with another monomer, and so on. This self-propagating reaction will continue if not inhibited by radical-termination, forming long polymer chains. Cross-linked networks result when the monomer is comprised of more than one reactive group [11,12]. The lifetime of radicals is limited by termination reactions. Termination occurs due to the reaction of two radicals (radical-radical recombination or *R-R* recombination) and the reaction of active centers with inhibitors [11–14]. Oxygen dissolved in the resin can act as an inhibitor by attaching to the growing radicals and producing less active peroxide radicals, which can hardly undergo chain propagation [11,12,15,16].

Typically, TPP systems employ a focused Gaussian beam moved by mechanical or optical means in a photocurable resin. Micro- and nanostructures are built via point-by-point scanning on each predetermined layer. The resin is almost transparent to the laser wavelength to allow deep penetration, so TPP is in principle capable of printing complex

^{*} Correspondence to: 2075 Rathbone Hall, Carl R. Ice College of Engineering, 1701B Platt St., Manhattan, KS 66506, USA. *E-mail address:* meng@ksu.edu (M. Zhang).

¹ Currently at Department of Mechanical & Industrial Engineering, University of Wisconsin-Platteville, Platteville, Wisconsin 53818, USA.

micro- and nanostructures in the resin volume without any support. A major disadvantage of TPP is that throughput is slow because the polymerized volume element ("voxel") is small, and a large number (10^4-10^7) of low-energy laser pulses are needed to polymerize every voxel [5–7,17]. To increase both the resolution and the throughput of TPP, research effort has focused on engineering the laser beam wavefront as a flexible and effective means for fabricating complex forms in a single or reduced number of exposures. Beam shapes can be designed and optimized for specific types of fabrication. Several shaped beams, including multiple beam spot array, helical-wavefront beams, ring-Airy beams, and Bessel beams, have been explored for rapid fabrication of functional structures in TPP [18–22]. A Bessel beam is employed in this work because the non-diffractive focus of Bessel beam can have the depth of field significantly longer than the Rayleigh range of a Gaussian beam of a comparable diameter.

Previous studies mainly utilized laser parameters in the weak-pulse regime, where single pulse energies are on the order of 1 nJ. In this regime, a large number of pulses are needed to polymerize the material, so repetition rates are high, up to 100 MHz [23]. With TPP, the probability $p_{\rm (abs)}$ for a photoinitiator to absorb two-photons increases with the square of the photon flux φ . Muller et al. estimate this probability can be as low as 0.02% under the relevant irradiation condition [24,25]. The present work considers the strong-pulse regime of TPP, where the laser is operated at low repetition rates (<< 1 MHz) and the pulse energies are high (>> 1 nJ). Because $p_{\rm (abs)} \propto \varphi^2$, two-photon absorption becomes much more efficient with strong pulses (μ J).

This research attempts to answer the following question: For a given photopolymer composition and a laser system with an average input laser power P, what is the most energy-efficient way of delivering the laser energy to create a single polymerized voxel? Energy-efficiency is key to improving fabrication throughput in a process constrained by total optical power. Results show that 3D structures can be fabricated using a few exposures of strong pulses (μ J). It is more energy-efficient to use fewer and higher-energy pulses in low single pulse energy regime (< $10~\mu$ J), yet this trend reverses when termination by R-R recombination becomes more severe in the regime of high single pulse energy ($10~\mu$ J - $30~\mu$ J). TPP fabrication in this regime can overcome some fundamental challenges faced by current high-repetition-rate systems, such as low throughput, elevated temperature, beam distortion, and obstruction by previously written structures.

2. Model development for two-photon polymerization by a bessel beam

Modeling TPP is fundamentally complex because of the spatial confinement, non-linear light-matter interaction, photochemistry, chemical kinetics, and the ultrashort pulsed nature of the laser source. Limited modeling work of TPP can be found in the literature [26,27]. Serbin et al. present a steady-state, free-radical-polymerization model that neglects radical-radical quadratic termination between pulses. Uppal et al. use constants for the chain propagation k_p and the quadratic termination k_t as polymerization progresses; however, k_p and k_t have been shown to depend on monomer conversion and temperature, and both decrease as polymerization progresses [15,28,29].

Here we present a mathematical framework to model TPP initiated by non-diffractive Bessel beams which captures the key light-matter interactions, including the polymerization kinetics under highly confined spatiotemporal scales. The high aspect-ratio of the Bessel beam allows us to simplify our analysis to only the radial direction. In addition, we are trying to understand the fabrication of the fiber-like polymerized structures reported in our previous work [17]. Therefore, we use the Bessel beam in this study.

The employed Bessel beam profile is shown in Fig. 1, and parameters of the model are collected in Table 1. Many aspects of the model are kept generic with respect to the specific chemistry used for TPP, and it is readily adaptable to other material systems. To generate results presented in this work, the model is applied to a specific material system consisting of 98 wt.-% pentaerythritol triacrylate (PETA) and 2 wt.-% photoinitiator (Irgacure® 819). Their molecular structures are shown in Fig. 2. Both PETA and Irgacure® 819 are widely available and commonly used in commercial and non-proprietary photopolymer formulations. PETA and Irgacure® 819 have also been used for TPP [30, 31].

The spatio-temporal evolution of various species is described by Eq. (1), and (3–5). The first term on the right side of each equation represents molecular diffusion. The consumption of the photoinitiator is given by Eq. (1), expressed in Cartesian coordinates. In TPP, the decomposition of photoinitiator depends on the square of local photon flux φ , represented by the second term on the right side.

$$\frac{\partial PI}{\partial t} = d_{PI} \left(\frac{\partial^2}{\partial x^2} + \frac{\partial^2}{\partial y^2} + \frac{\partial^2}{\partial z^2} \right) PI - \psi \delta \varphi^2 PI$$
 (1)

$$\varphi = \frac{I}{h\nu} \tag{2}$$

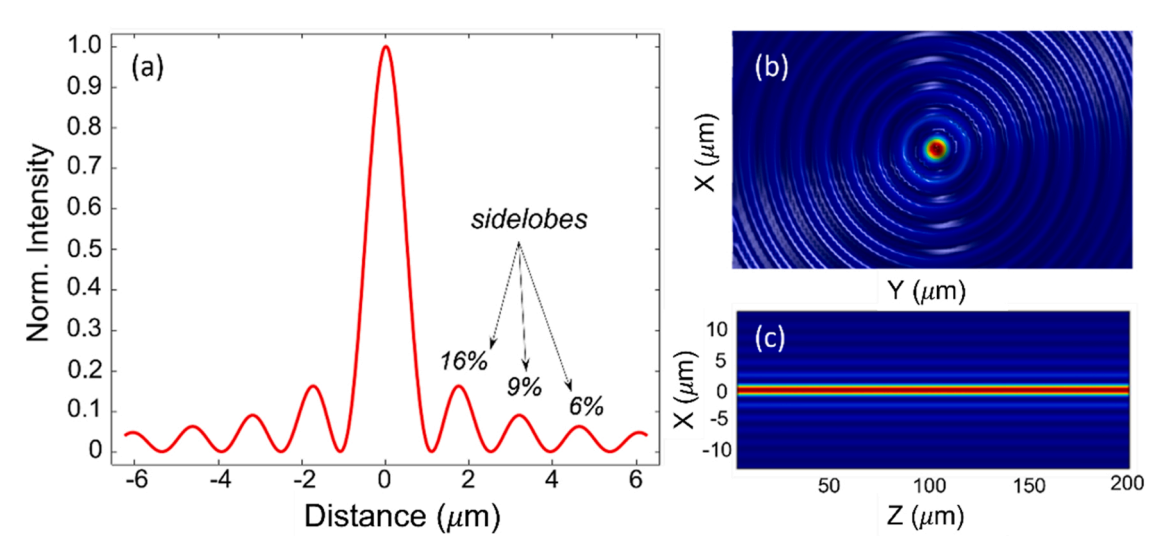


Fig. 1. (a) Radial intensity distribution of a Bessel beam. (b) Transverse section of a Bessel beam. (c) Longitudinal section of a Bessel beam.

Table 1Laser parameters and materials properties of the TPP system.

Parameter	Description	Value	Unit	Ref.
τ	Pulse duration	170	fs	
f	Repetition rate	0.1 - 100	kHz	
$E_{\rm p}$	Pulse energy	0.5-30	μJ	
λ	Wavelength	515	nm	
ω_0	Beam radius	0.88	μ m	
δ	Two photon cross section	5	GM	[32]
Ψ	Quantum yield	0.42		[33]
α	Absorbance of UV cured PETA at 515 nm	0.115	cm ⁻¹	measured
I_0	Peak intensity	$10^{15} - 10^{17}$	W m ⁻²	
$d_{ m j0}$	Pre-exponentiel diffusion constant ($j = PI, R, M$)	3.26×10^{-10}	$m^2 s^{-1}$	[15]
$d_{\rm OX}$	Diffusion constant for oxygen	2.27×10^{-10}	$m^2 s^{-1}$	[15]
$k_{\mathrm{p}0}$	Pre-exponential propagation constant	2.4×10^6	m ³ mol ⁻ 1 s ⁻¹	[15]
$k_{ m t0}$	Pre-exponential termination constant	3.59×10^{5}	m ³ mol ⁻ 1 s ⁻¹	[28]
$k_{ m q}$	Quenching constant	2.3×10^3	m ³ mol ⁻ 1 s ⁻¹	[28]
E_{pa}	Propagation activation constant	30000	J mol ⁻¹	[30]
$E_{\rm ta}$	Termination activation constant	22000	J mol ⁻¹	[29]
$E_{\rm a}$	Diffusion activation constant	22000	J mol ⁻¹	[29]
M_0	Monomer double bond concentration	11868	mol m ⁻³	
PI_0	Photoinitiator concentration	132	mol m ⁻³	
O_{20}	Oxygen concentration	6	mol m ⁻³	[15]
ρ	Resin density	1190	kg m ⁻³	
C	Resin heat capacity	1870	J kg ⁻¹ K ⁻	
k	Resin thermal conductivity	0.142	W m ⁻¹ K ⁻¹	
Н	Enthalpy of polymerization	-54800	J mol ⁻¹	[34]

Here, PI, ψ , and δ represent the concentration, chemical quantum yield, and two-photon absorption cross section of the photoinitiator, respectively. The term $d_{\rm PI}$ is its molecular diffusion constant, which varies both spatially and temporally due to temperature distribution. I is the laser intensity distribution, h is the Planck constant, and ν is the optical frequency.

The evolution of the radical concentration R is described by Eq. (3). The second term on the right denotes the generation of radicals due to photoinitiation. The other terms describe termination reactions due to R-R recombination and quenching by oxygen, having local concentration O_2 .

$$\frac{\partial R}{\partial t} = d_R \left(\frac{\partial^2}{\partial x^2} + \frac{\partial^2}{\partial y^2} + \frac{\partial^2}{\partial z^2} \right) R + \psi \delta \varphi^2 P I - 2k_t R^2 - k_q O_2 R$$
(3)

Here, $d_{\rm R}$ is the radical diffusion constant, and $k_{\rm t}$ and $k_{\rm q}$ are R-R recombination termination and oxygen-quenching constants, respectively.

Eq. (4) describes the spatio-temporal change in \mathcal{O}_2 caused by oxygen quenching.

$$\frac{\partial O_2}{\partial t} = d_{O_2} \left(\frac{\partial^2}{\partial x^2} + \frac{\partial^2}{\partial y^2} + \frac{\partial^2}{\partial z^2} \right) O_2 - k_q R O_2 \tag{4}$$

Eq. (5) describes the consumption of monomer due to chain propagation, where $k_{\rm p}$ is the propagation constant. TPP is most often performed using multi-functional monomers that can cross-link, like PETA. In that case, monomer is tracked as the concentration of reactive monomer-groups, M. PETA, the monomer studied in this work, has three reactive acrylate groups, so the initial concentration M_0 is three times the molecular concentration of PETA.

$$\frac{\partial M}{\partial t} = d_M \left(\frac{\partial^2}{\partial x^2} + \frac{\partial^2}{\partial y^2} + \frac{\partial^2}{\partial z^2} \right) M - k_p R M \tag{5}$$

During TPP, the temperature T of the photocurable resin can increase due to absorption of laser light and the exothermicity of polymerization [27]. The spatial-temporal distribution of temperature within the resin is given by Eq. (6).

$$\rho C \frac{\partial T}{\partial t} = k \left(\frac{\partial^2}{\partial x^2} + \frac{\partial^2}{\partial y^2} + \frac{\partial^2}{\partial z^2} \right) T - H \frac{\partial M}{\partial t} + c\alpha I$$
 (6)

$$c = 1 - \frac{M}{M_0} \tag{7}$$

The constants ρ , C, and k are the resin's density, specific heat capacity, and heat conductivity, respectively. H is the change in enthalpy from polymerization. Parameter c is the monomer conversion, or fraction of reacted monomer.

The dominant source of linear absorption, quantified by α , results from the cured photopolymer. Experimental measurements performed for this work and reports by others [32,34] confirm that PETA and Irgacure® 819 have very low absorption at 515 nm, so these sources of linear absorption are ignored. The photopolymer, however, yellows upon photocuring, as is commonly observed for other formulations. Yellowing is commonly attributed to absorbing species that form upon photodecomposition of the initiator [35]. Other works investigated damage that can occur during TPP adjacent to previously patterned features and attributed it to linear absorption by the photocured material [36]. For the present work, α of the photocured resin was determined experimentally. Eq. (6) then weights the amount of linear absorption in proportion to the degree of polymerization, as expressed by the degree of conversion c in Eq. (7). As shown below, linear absorption could be neglected overall in this work because heat generated in the focal volume is overwhelmingly dominated by exothermicity of the polymerization reaction. The low absorptivity of the material permits the laser intensity to be regarded as undepleted throughout the interaction volume.

The propagation and termination constants k_p and k_t have an Arrhenius temperature dependence. They are functions of monomer conversion c, as given by Eqs. (8) and (9), which are extrapolated based on published experimental measurements [15,28–32]. The molecular diffusion d_i (where i = PI, R, M) is also temperature dependent, per Eq. (10). The diffusivity of oxygen is assumed to be a constant [15].

$$k_p = k_{p0} exp\left(\frac{-E_{pa}}{R \cdot T}\right) \cdot 10^{-(5.115 \cdot c^2 + 0.472 \cdot c)}$$
 (8)

(a) O O (b)
$$H_3C$$
 CH_3 H_3C CH_3 CH_3 CH_3 CH_3 CH_3 CH_4 CH_5 CH

Fig. 2. Chemical structures of (a) pentaerythritol triacrylate (PETA) and (b) phenylbis(2,4,6-trimethylbenzoyl) phosphine oxide (Irgacure® 819).

$$k_t = k_{t0} exp\left(\frac{-E_{ta}}{R \cdot T}\right) \cdot 10^{-(3.892 \cdot c^2 + 1.9538 \cdot c)}$$
(9)

$$d_i = d_{i0}exp\left(\frac{-E_a}{R[T]}\right)(i = PI, R, M)$$
(10)

The constants $k_{\rm p0}$ and $k_{\rm t0}$ are pre-exponential factors, $E_{\rm pa}$ and $E_{\rm ta}$ are the activation energies for monomer and radicals, $d_{\rm i0}$ is the diffusion constant, and $E_{\rm a}$ is the activation energy for diffusion. Fig. 3 illustrates how the propagation, termination, and diffusion constants change as a function of temperature and monomer conversion c.

3. Numerical methods

The finite element method (FEM) for modeling TPP was implemented in COMSOL Multiphysics. This model employs a fixed (Eulerian) discretized mesh spanning the domain as shown in Fig. 4. Finer meshes are applied to the laser irradiated region, and coarser meshes are used in the other areas which are of less interest.

The selection of mesh size is important. The mesh must be able to achieve accurate results while balancing between element size and computation time. To determine the optimal element size, a mesh convergence analysis was performed under the conditions of 1 kHz and 6 μ J. As demonstrated in Fig. 5, when the element size is smaller or equal to 0.1 μ m, the computed results (PI and R concentration) converge to a repeatable solution with decreasing element size. So, the element size of 0.1 μ m is applied to the laser irradiation region as additional refinement is unnecessary after reaching mesh independence.

In addition to the mesh size, the time-stepping algorithm plays an important role in the fidelity and efficiency of computation. An implicit time-stepping algorithm installed in COMSOL Multiphysics was used to solve the time-dependent problem. The algorithm chooses a time step based upon a user-specified relative tolerance. Loose tolerance can skip over certain transient events, while tight tolerance might take up too much computational resource. To accurately and efficiently model femtosecond laser irradiation with pulse duration on the order of 170 fs, an *Events Interface* in COMSOL Multiphysics was used to force a solution evaluation when the pulse switches on at a known laser frequency. So, small time steps are taken immediately after the events to give good resolution of the variation, and large time steps are taken when the laser irradiation is off to minimize the overall computational cost.

The Backward Differentiation Formula (BDF) is implemented to solve the ordinary differential equations given in Section 2. The simulated results are presented and discussed in sections that follow. Section 4 depicts evolution of species and temperature under the conditions of 1 kHz repetition rate and 6 μ J pulse energy. Section 5 compares predicted feature size with experimental measurement for model validation. Section 6 discusses the most energy-efficient way of delivering the laser energy to create a single polymerized voxel.

4. Evolution of species and temperature in TPP at 1 kHz repetition rate

4.1. Photoinitiator

Fig. 6(a) depicts the temporal change of the concentration of photoinitiator at the center of the Bessel beam irradiation. Given that the Bessel beam is non-diffractive, the species concentration along the direction of beam propagation (z) is assumed to be constant. The photoinitiator concentration decreases with each laser pulse and remains almost unchanged during the dark period because diffusion of the photoinitiator is negligibly small. The reduced photoinitiator concentration at the end of each dark period becomes the initial condition for the next pulse, which affects the number of radicals generated and eventually the polymerization kinetics. Overall, the photoinitiator concentration decays at a rate that depends on the square of the peakintensity I_0 and follows the envelope of $\exp(-\psi \delta \tau_{\exp}(I_0/\hbar \nu)^2)$. Here, $\tau_{\rm exp} = N/f$ is the total time elapsed after exposure with N pulses. Fig. 6(b) demonstrates that the spatial distribution of the photoinitiator correlates with the beam intensity profile. For instance, the photoinitiator is depleted rapidly at the center lobe of the Bessel beam (x = 0), where the laser intensity is the highest. No photoinitiation occurs in the valleys between concentric rings of the Bessel beam where the intensity is zero.

4.2. Radical

The temporal and spatial distributions of radicals define the volume where polymerization takes place. Fig. 7(a) demonstrates that the concentration of radicals at the center of the Bessel beam increases with decomposition of the photoinitiator by laser irradiation. The generated radicals decay rapidly till the next pulse arrives due to R-R recombination and quenching by oxygen. Polymerization does occur during this period but does not change the concentration of radicals because addition of monomer merely propagates the radical. Fig. 7(b) shows the spatial distribution of radical concentration. At the end of 1 ms and 5 ms, the maximum radical concentration appears at the center of the focal volume because of high laser intensity and the accumulation of radicals. In contrast, a double-peaked curve is observed at the end of 25 ms, implying that radical concentration at the center of Beam drops compared to the immediate vicinity where the intensity is lower. This change is caused by R-R termination, which is strongest at the center of the beam where the laser intensity is highest. In this region, the radical concentration drops rapidly during the dark period, whereas areas with lower radical concentration do not experience significant R-R recombination. This phenomenon indicates that high laser intensities could lead to the inefficient utilization of radicals.

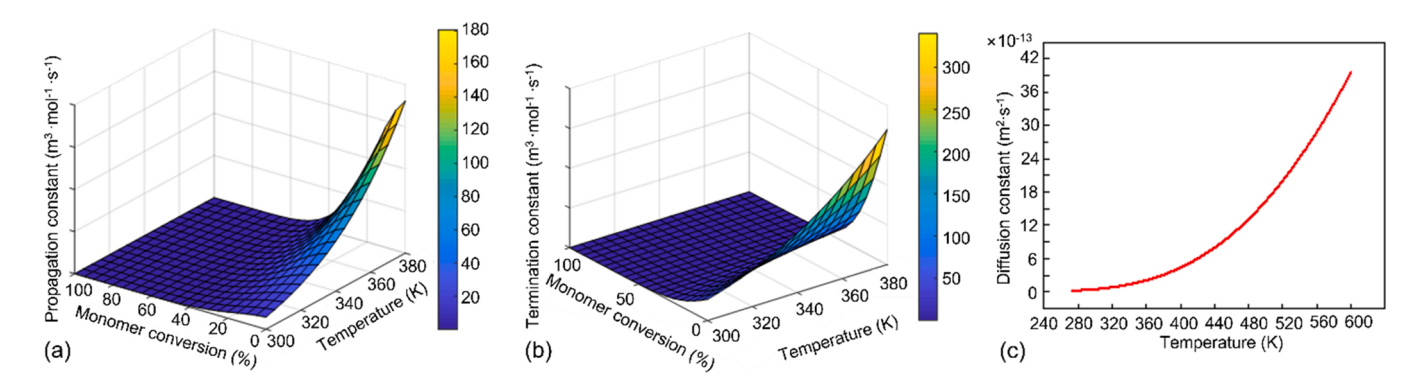


Fig. 3. Dependence of (a) propagation and (b) termination constants on monomer conversion and temperature. (c) Dependence of molecular diffusion on temperature.

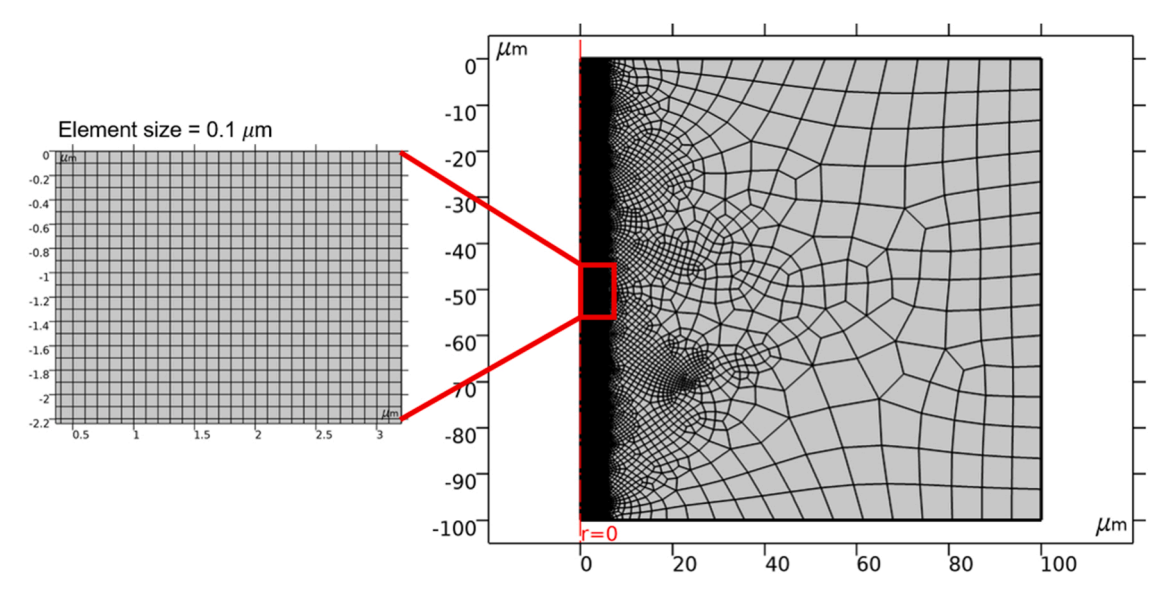


Fig. 4. A customized mesh, which contains more mesh elements around the irradiated volume.

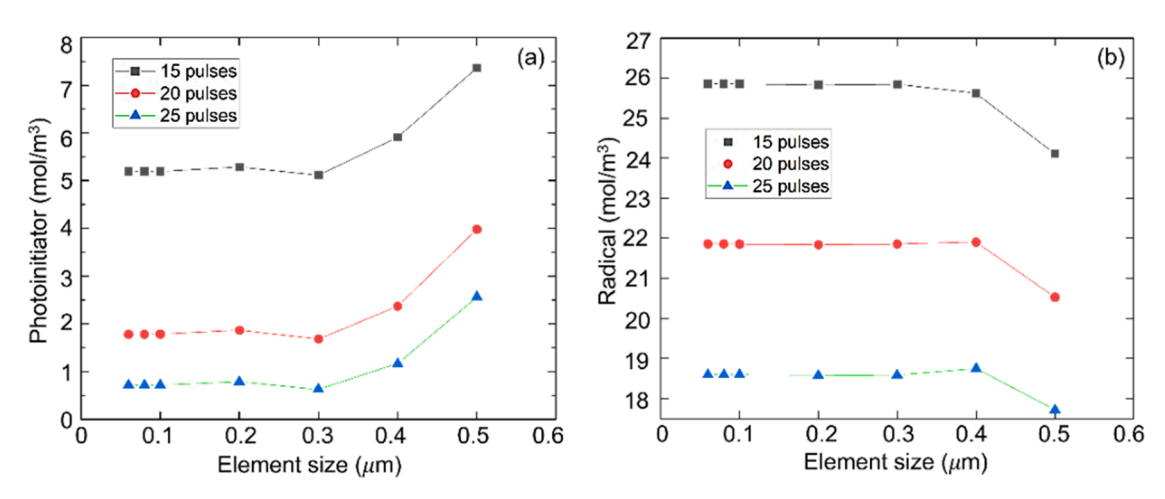


Fig. 5. Results from an analysis of mesh-convergence.

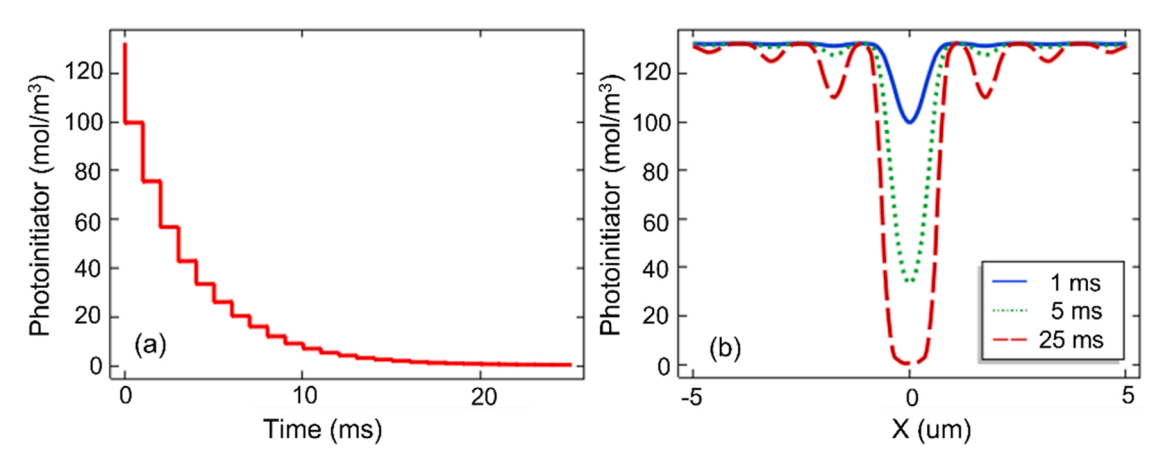


Fig. 6. (a) The temporal evolution of photoinitiator concentration (f = 1 kHz, $E_p = 6 \mu J$) at the center of the Bessel beam (x = 0). (b) The photoinitiator concentration along the radial direction at three times after start of the exposure.

4.3. Oxygen

Fig. 8(a) shows that oxygen is rapidly depleted around the focal

region due to rapid quenching and diffusion. Radicals generated by the first pulse consume all oxygen inhibitors, enabling polymerization to begin. Oxygen molecules are then replenished by diffusion into the

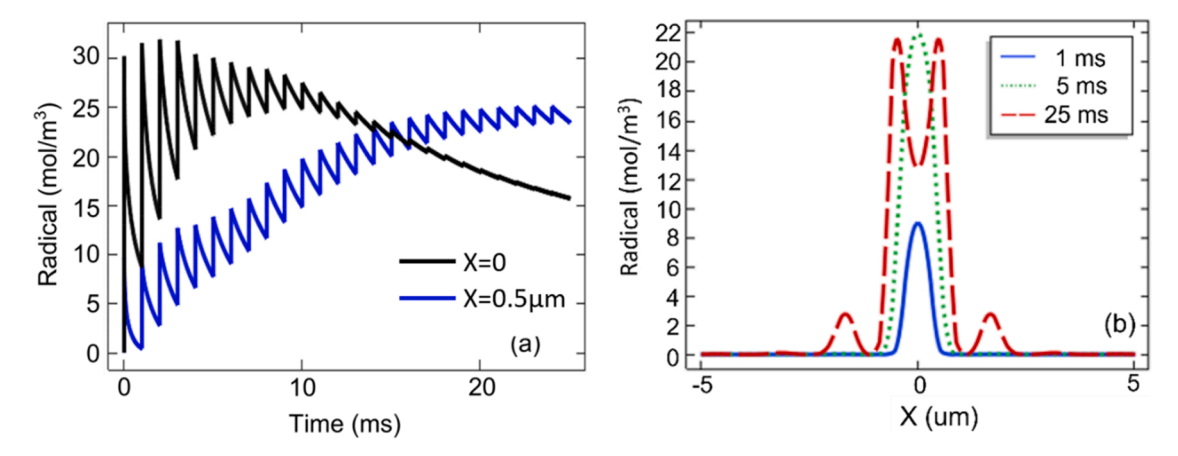


Fig. 7. (a) The temporal evolution of radical concentration (f = 1 kHz, $E_p = 6$ μ J) at the center (x = 0) and off-center (x = 0.5 μ m) of the Bessel beam. (b) Radical concentration along the radial direction at three times after start of the exposure.

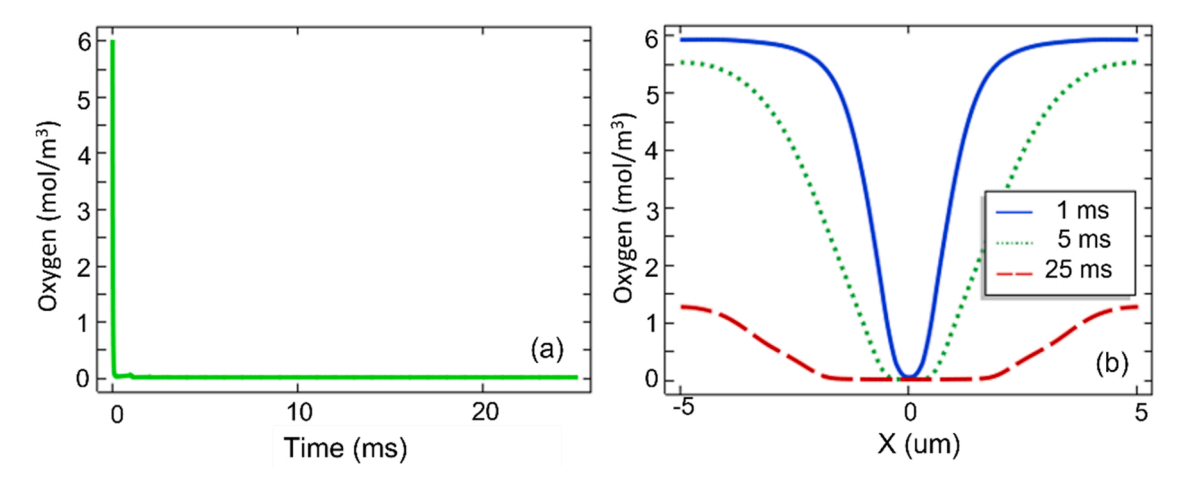


Fig. 8. (a) The temporal evolution of oxygen concentration (f = 1 kHz, $E_p = 6 \mu \text{J}$) at the center of the Bessel beam (x = 0). (b) Oxygen concentration along the radial direction at three times after start of the exposure.

irradiated volume. As shown in Fig. 8(b), the oxygen depleted region broadens with subsequent pulses. The most severe oxygen depletion occurs at the center lobe, whereas the oxygen is only partially consumed in the vicinity. Diffusion drives oxygen from the surroundings into the irradiated volume and decreases the concentration gradient.

4.4. Monomer

Fig. 9(a) shows the temporal profile of monomer concentration and

%-conversion to polymer. The rate of monomer consumption is high at first, but it decreases with each pulse. The shape of the polymerized voxel is defined by the area that exceeds a critical conversion threshold value. In these simulations, the threshold was taken to be 60%. The threshold value was determined by Raman spectroscopy of polymerized features that were sufficiently robust to withstand the developing process. The contour obtained from the monomer conversion plot (Fig. 9 (b)) can be used to predict the dimension of a polymerized structure, based on which the model can be compared to experimental results.

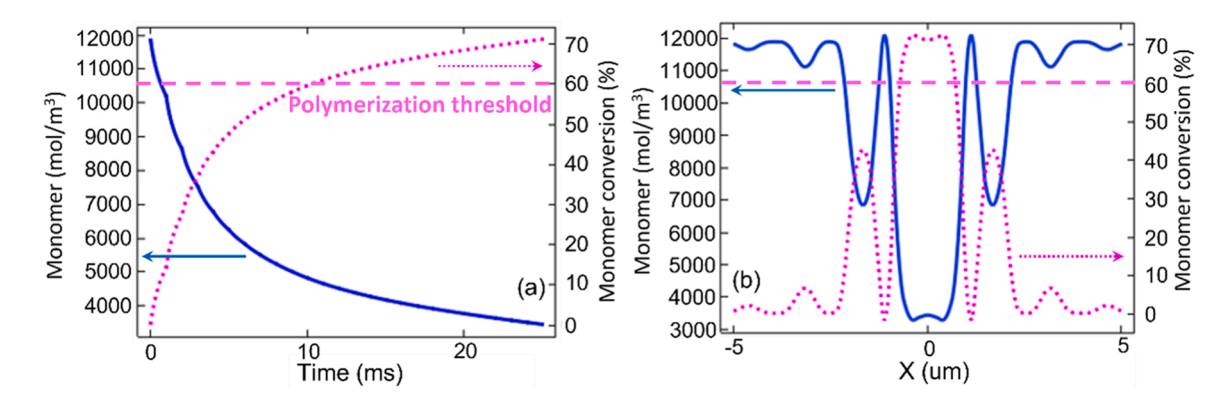


Fig. 9. (a) The temporal evolution of monomer concentration/conversion (f = 1 kHz, $E_p = 6 \mu J$). (b) The monomer concentration/conversion along the radial direction (data extracted 25 ms after laser exposure). The horizontal dashed lines represent the 60% polymerization threshold.

4.5. Temperature

Fig. 10 is a double Y-axis plot. The left axis gives temperature, which increases due to exothermic polymerization and absorption of laser energy. The right axis is the rate of monomer conversion, dM/dt.

The monomer conversion rate jumps with each laser pulse, and then rapidly drops. The conversion rate drops between laser pulses due to the combined effects of oxygen quenching, *R-R* recombination, and slowing of the propagation rate per Eq. (8). Each of these effects contributes to varying amounts over the total exposure time. For example, oxygen quenching is only significant for the first pulse, but insignificant thereafter because oxygen is locally depleted. With each subsequent pulse, more radicals are formed, so the conversation rate rises again. But the rise is less than for earlier pulses because the concentration of photonitiator steadily decreases with each pulse, and it is not replenished by diffusion (Fig. 6). After about 10 pulses, the photoinitiator is consumed, so the rate of monomer conversion simply decreases with time.

Throughout irradiation, the temperature change is modest, and the overwhelming majority of heating results from the exothermicity of polymerization. Heating due to absorption of laser light increases the temperature by no more than $\sim\!0.03$ K (see inset), because two-photon absorption is weak, and the material has negligible one-photon absorption. Eq. (6) is configured to track linear absorption from the polymer, as this was found experimentally to be dominant. Because monomer conversion c increases throughout the exposure, heating due to laser absorption actually increases continuously. The temperature increases due to absorption are overwhelmed by heating from polymerization, and even that rises by no more than 4 K, reaching a peak of 296.8 K after approximately 10 pulses. As the polymerization slows, heat within the irradiated volume diffuses to the surroundings, and the temperature drops.

Similar results were reported by Mueller et al. The authors experimentally measured temperature in situ within the irradiation volume during TPP and found it rose by no more than approximately 5 K under relevant fabrication conditions ($P \le 10$ mW, effective exposure time = 20 ms) [37]. When the volume is overexposed, causing damage, much higher temperature increases result (100–300 K) [37]. Micro-explosions (bubble formation due to boiling of monomer) have also been reported elsewhere [37]. The sudden rise in temperature has been attributed to nonlinear process like photoionization and formation of plasma. These effects are not modeled in the present work.

5. Model validation

The experimental setup to validate the model has been described previously [17]. The laser source is a femtosecond laser (Pharos, Light Conversion, Lithuania) delivering 170 fs laser pulses at a wavelength of 1030 nm. The laser beam then passes a second harmonic generation module, and the 515 nm laser beam is used for TPP. The 515 nm laser beam is focused by an axicon (Doric Lenses Inc., Canada) with a base angle of 25° to create a Bessel beam with a narrow center lobe ($< 2 \mu m$ in diameter) and a long depth of focus (> 10 mm). To verify the model predictions, high aspect ratio pillar structures were fabricated using the Bessel beam with P = 5-22 mW and pulse numbers of 20-50 pulses at 1 kHz repetition rate in a commercial acrylic resin (3D ink, USA). The 3D ink resin consists of > 98 wt.-% acrylic monomer and < 2 wt.-% The model is applied to a specific material system consisting of acrylic monomer 98 wt.-% pentaerythritol triacrylate (PETA) and 2 wt.-% photoinitiator (Irgacure® 819), which closely resembles the resin used in experiments. After laser exposure, polymerized structures were rinsed with isopropyl alcohol to remove uncured resin and then dried. Developed pillar structures were examined with SEM (Ultra 55 FEG, Carl Zeiss AG, Germany) for imaging and measurement. The predicted size of a polymerized structure was determined by the polymerization threshold line (60%) as illustrated in Fig. 11.

Fig. 12 shows the comparison between SEM-measured and model-predicted polymerized pillar structure diameters. In general, measured pillar diameters increase with *P*, although there are some fluctuations observed at high laser power due to experimental variance. The simulation, entirely driven by parameters adopted from the literature [15, 28–33], manage to estimate pillar structure diameters that are comparable, within one order of magnitude, to the experimental measurements.

The stepwise behavior of the diameter growth presented in the predictions in Fig. 12 is caused by the polymerization of Bessel beam side lobes. As shown in Fig. 1, the first, second, and third side lobes are 16%, 9%, and 6% of the peak intensity of the central lobe. These side lobes can also polymerize the photocurable resin during TPP once exceeding the polymerization threshold (60%). For instance, at the end of 50th pulse (Fig. 12(d)), the predicted diameter gradually grows from 1.33 μ m to 1.65 μ m as P increases from 5 mW to 8 mW, then the diameter abruptly jumps to 3.78 μ m when the P increases to 10 mW. This phenomenon is attributed to the polymerization caused by the first side lobe. The second jump of diameter occurs at P=18 mW due to the

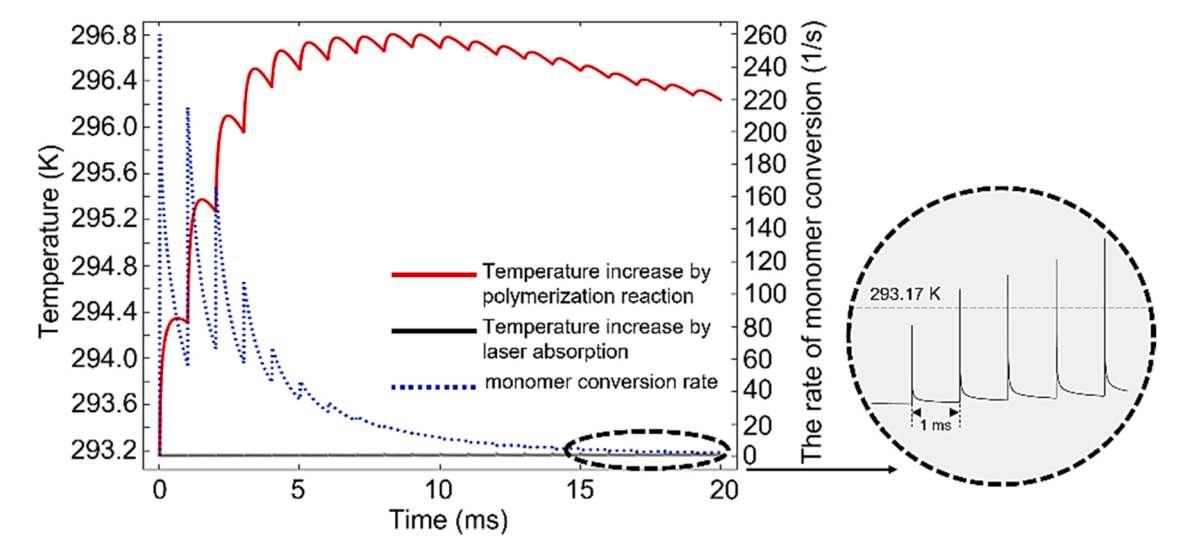


Fig. 10. Temperature increase versus time caused by exothermicity of polymerization (solid red curve) and laser absorption (solid black curve). The rate of monomer conversion versus time is plotted as the dotted blue curve (f = 1 kHz, $E_p = 6 \mu \text{J}$).

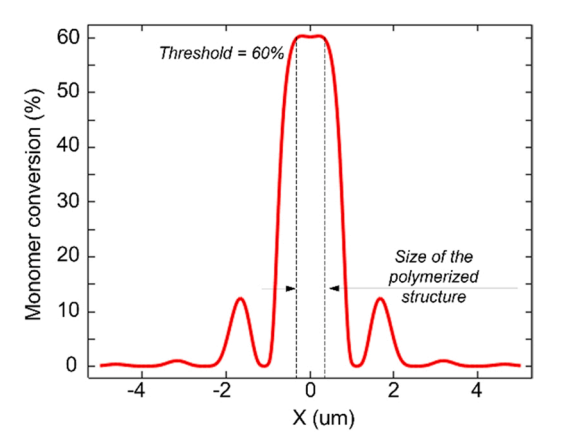


Fig. 11. Predicted size of a polymerized feature assuming polymerization threshold is 60% monomer-conversion.

polymerization caused by the second side lobe of the Bessel beam. Similar observations are also found in experimental measurements highlighted in Fig. 12(d).

6. Results and discussion

6.1. Polymerization time and energy demand under different irradiation conditions

A key research thrust in TPP is to substantially decrease polymerization time without compromising TPP's sub-micrometer resolution. Here, polymerization time is the time needed for the monomer conversion at the center of exposure to exceed the polymerization threshold. This is different from the "fabrication time" to form a certain type of structures. We use this definition of polymerization time because our study focuses on when polymerization starts for a given set of exposure conditions. Fig. 13(a) plots the behavior of polymerization time needed to polymerize a single voxel by reaching its photopolymerization threshold (60%) under laser irradiation conditions of different single pulse energy levels (up to 15 μ J) and repetition rates (up to 100 kHz). The plot exhibits a saddle shape. A collection of laser irradiation conditions that yield the shortest polymerization time can be found in the valley region of this plot. The valley region is axisymmetric about the origin and the (15 μ J, 100 kHz) line. Under conditions of low pulse energy and low repetition rate, polymerization time increases due to termination by oxygen inhibition. The oxygen dissolved in the resin acts as a quencher by attaching to both the primary radicals and propagating radicals. They yield fewer active peroxide radicals, which cannot participate in further polymerization reactions. The number of generated radicals is significantly reduced under irradiation conditions of low laser energy and lower repetition rate. They are immediately scavenged

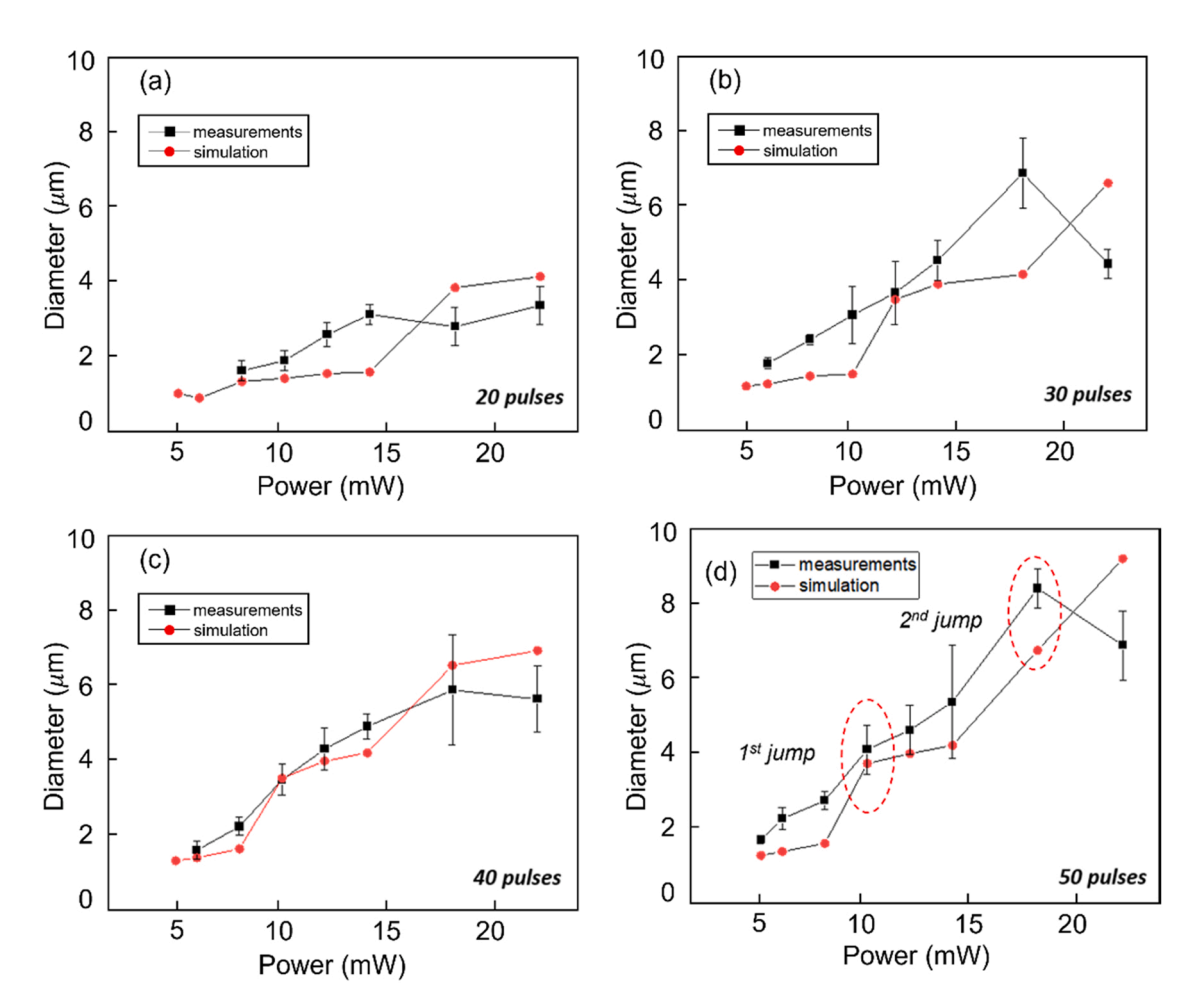


Fig. 12. Comparison of pillar-diameters determined from experiment and simulation versus average input power P for various numbers of total pulses. Laser repetition rate is 1 kHz. The error bars are plotted at the level of \pm 1 standard deviation of the means. The width of each fiber-like polymerized structure was measured at least three times at the top, middle and bottom portions of the polymerized structure.

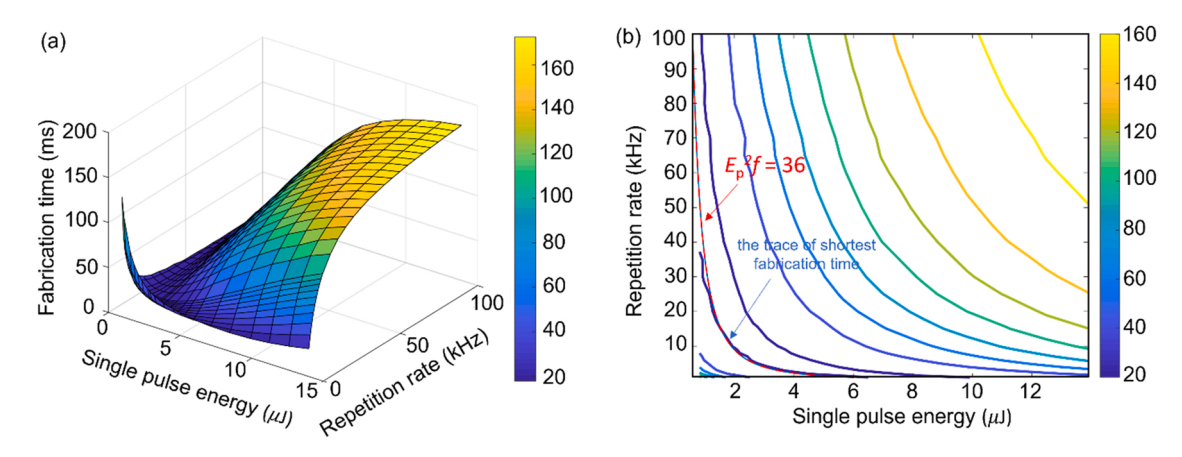


Fig. 13. (a) Polymerization time needed to polymerize a single voxel under different laser irradiation conditions. (b) Contours of identical polymerization time obtained under a set of laser irradiation conditions having $E_n^2 f = Constant$.

by oxygen and make no contribution to polymerization reaction. As a consequence, oxygen quenching slows down polymerization reaction as the chain reaction will not be able to propagate until the oxygen molecule concentration is greatly reduced [15,38]. When TPP is performed under irradiation conditions with high single pulse energy and high repetition rate, the vast majority of the generated radicals become wasted (Fig. 16), as the quadratic *R-R* recombination terminates the chain propagation, so that polymerization time is lengthened as well.

Fig. 13(b) shows that identical polymerization time can be obtained under a set of laser irradiation conditions that satisfy $E_p^2 f = \text{Constant}$, where E_p is pulse energy (μJ), f is repetition rate (kHz). This relation can be interpreted as that equal absorbed total energy $(E_p^2 f)$ contributes to similar polymerization time. The power of two in $E_p^2 f$ comes from the nonlinearity of two photon absorption. Radicals are generated by the decomposition of the photoinitiators that undergo laser irradiation at the focal volume. The decomposition rate of photoinitiators depends on the square of applied photon flux φ , which is proportional to the applied laser intensity *I* and single pulse energy given a constant pulse duration. For instance, the trace of shortest polymerization time (19 ms) corresponds to the relationship of $E_p^2 f = 36$, which is plotted as the red dotted curve in Fig. 13(b), so all the combinations of single pulse energy and repetition rate on the dark blue trace yield similar polymerization time. For instance, a voxel can be polymerized in 19 ms by an irradiation of $0.6 \mu J$ single pulse energy at 100 kHz repetition rate (1900 total pulses), and the same polymerization time can also be achieved by an irradiation of 6 μ J single pulse energy at 1 kHz repetition rate (19 total pulses).

In addition to decreasing polymerization time, it is also important to explore the most energy-efficient way of delivering the laser energy to achieve a single polymerized voxel. It is found that the energy demands

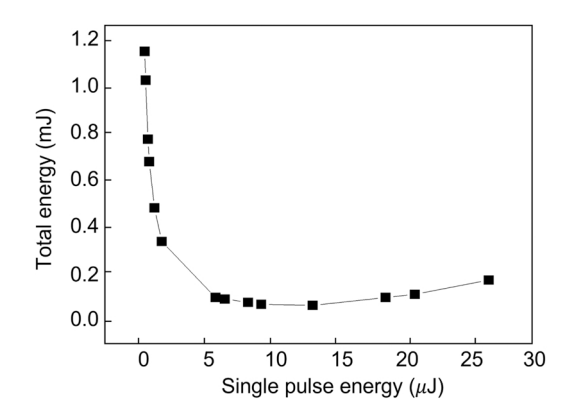


Fig. 14. The total energy under a set of laser irradiation conditions ($E^2f=36$) that yield shortest polymerization time.

on each iso-polymerization time contour ($E_p^2 f = Constant$) are different. Fig. 14 depicts the energy demand under a set of laser irradiation conditions ($E_p^2 f = 36$) that yields the shortest polymerization time. It is observed that when single pulse energy is lower than 10 μ J, energy demand decreases as single pulse energy increases; however, when single pulse energy increases beyond 10 μ J, the opposite trend is displayed because of the strong termination caused by R-R recombination. It's important to understand that all points shown in Fig. 14 correspond to the same fabrication time (19 ms). Under these conditions of $E_n^2 f$ = 36, the irradiation condition that minimizes the total energy is most efficient in energy use for a given polymerization time. Time needed to fabricate an entire structure is outside the scope of the current work and will be a topic of future study. While the exact values vary in different TPP systems, Fig. 14 shows that in a process where the total laser energy is the constraint, there exists an optimal combination of pulse energy and repetition rate, which yields the lowest total laser energy to fabricate a single voxel. Fig. 14 is in agreement with experimental data reported in the literature [39] with small pulse energy when R-R recombination is insignificant (see Supplemental Materials for a detailed comparison and analysis). It should be pointed out that in practice, optical breakdown and damage of the photopolymer may prevent access to the R-R recombination regime. Therefore, Fig. 14 should be viewed as an ideal case for materials that have sufficiently large "dynamic range" or "processing window" that photopolymerization occurs normally and pulse energy is high enough for R-R recombination to play a role, yet the pulse energy is below the level where optical breakdown or damage occurs.

6.2. Influence of quadratic radical-radical (R-R) recombination

To study the effect of R-R recombination, simulations were run with and without the term of $2k_tR^2$ in Eq. (3) (all other parameters are identical) and the concentration of radicals was plotted over 25 pulses. Under both conditions, the contribution of each laser pulse to creating additional radicals can be observed, but the step-like increase becomes less and less till reaching equilibrium as photoinitiator concentration decreases. The red dotted curve (W/O R-R recombination) continues to rise until it approaches the same concentration as that of the photoinitiator when reaction starts. The blue curve (W R-R recombination) has a sharp increase when one pulse arrives, and then decays rapidly and increases again when the next pulse is delivered. This comparison of trends indicates that a large number of the generated radicals can become wasted due to R-R recombination. The termination becomes more severe when a high radical concentration is present as indicated by the term of $2k_tR^2$ in Eq. (3). Fig. 15.

Fig. 16 shows radical waste percentage under different laser irradiation conditions. The repetition rate ranges from 100 Hz to 100 kHz,

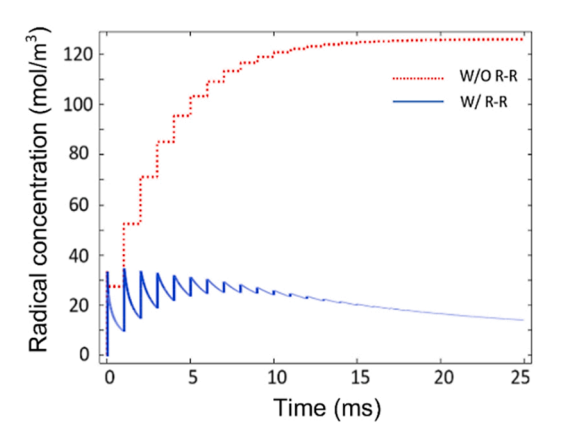


Fig. 15. The radical concentration with and without termination by radical-radical (*R-R*) recombination (6 μ J pulses and f = 1 kHz).

and the single pulse energy spans from $0.5~\mu J$ to $30~\mu J$. The waste percentage is calculated as the summation of all terminated radicals divided by the summation of all generated radicals during the entire polymerization time (the time it takes for a single voxel to reach its photopolymerization threshold). Fig. 16(a) shows the radical waste percentage at the repetition rate of 100 Hz. In the regime of single pulse energy below $10~\mu J$, radical loss is more severe at lower pulse energy due to scavenging of free radicals by oxygen quenching termination reactions. Whereas in the regime of stronger laser pulse $(10~\mu J - 30~\mu J)$, an increase of single pulse energy gives a higher percentage of radical waste (up to 98.87%), caused by the reaction of R-R recombination. Fig. 16(d) depicts the radical waste percentage at the repetition rate of 100 kHz. A

large number of pulses are delivered during the polymerization time and generate a decent number of radicals. However, it turns out that approximately 98% radicals are terminated when the single pulse is greater than 1 μ J due to the *R-R* recombination. Fig. 16(b) and 16(c) demonstrate radical waste percentage at the repletion rate of 1 kHz and 10 kHz, respectively. Overall, the majority of radicals (> 55%) are terminated by the reaction of *R-R* recombination, and an increase of single pulse energy gives a higher percentage of radical waste (up to 98.87%).

Fig. 17(a) shows how laser intensity influences monomer conversion for different numbers of pulses applied (1, 5, 10, 20, and 50 pulses). This set of simulations is conducted using a fixed repetition rate of 1 kHz, so the polymerization time to execute the pulse numbers are 1 ms, 5 ms, 10 ms, 20 ms, and 50 ms, respectively. Overall, for a given laser intensity, monomer conversion increases as more pulses are delivered. The same monomer conversion can be achieved by a larger number of low intensity pulses and also by fewer high intensity pulses. Fig. 17(a) also indicates that too few pulses (<< 20) cannot polymerize a voxel above the photopolymerization threshold (60%). For a fixed polymerization time, monomer conversion first rises as laser intensity increases, and then it decreases (or plateaus in the case of 1 pulse) as laser intensity continues to increase. This transition is believed to be the result of radical termination by the quadratic R-R recombination induced by high intensity laser pulses. A similar phenomenon is also observed in Fig. 17 (b), where the maximum monomer conversion doesn't occur at the peak laser intensity. This is because at high laser intensity, quadratic R-R recombination can take place that decreases the active radicals to react with monomer molecules. In this case, laser energy is utilized inefficiently when delivered as fewer high-intensity pulses.

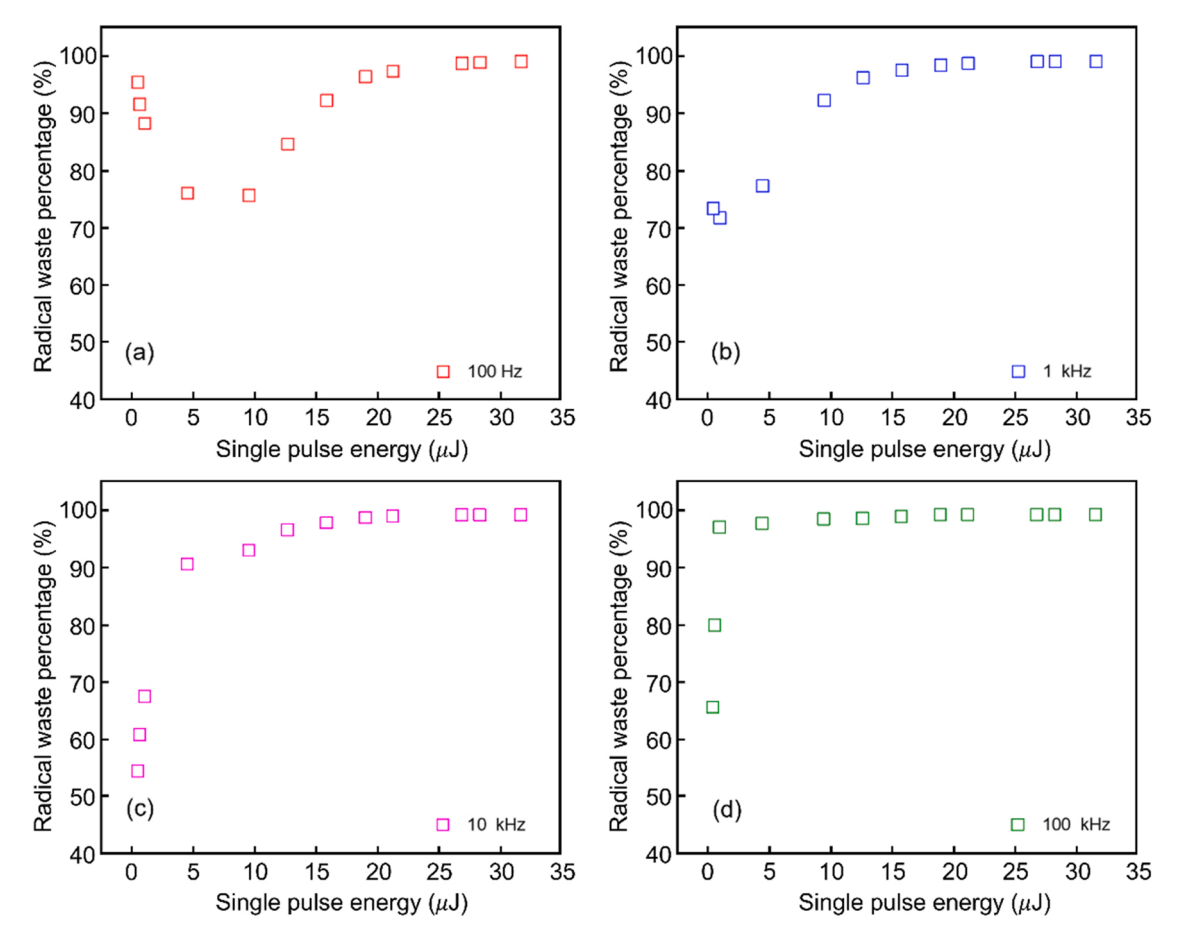


Fig. 16. Radical waste percentage under different laser irradiation conditions.

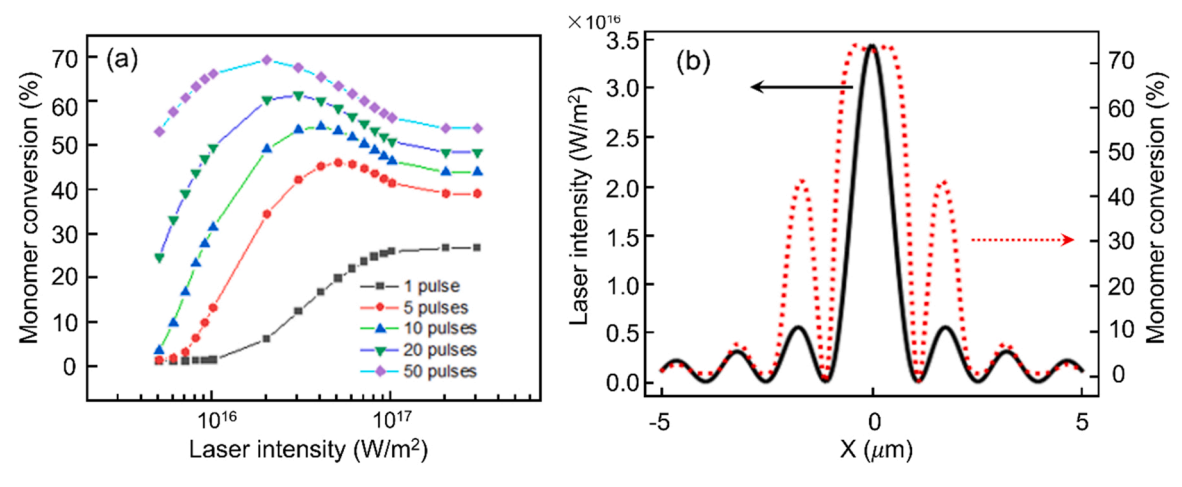


Fig. 17. (a) The influence of laser intensity on monomer conversion (number of pulses = 1, 5, 10, 20,and 50). (b) Monomer conversion along the radical direction (data extracted 20 ms after laser exposure).

7. Conclusions

This paper presents a mathematical framework to model TPP activated with Bessel beams under a wide range of pulse-repetition rates, energies, and spatio-temporal regimes. The investigated laser operational regime is different from a conventional megahertz repetition rate laser system. A femtosecond laser is operated with low repetition rate (0.1-100 kHz) and high peak intensity $(10^{15} \text{ W m}^{-2} - 10^{17} \text{ W m}^{-2})$. Results show that the number of pulses needed to polymerize a voxel in this regime is significantly lower than the ten thousand to ten million cumulative laser pulses needed by a megahertz repetition rate laser. The required polymerization time is also shortened while maintaining the superb sub-wavelength feature resolution of two-photon polymerization. Sub wavelength structures (400 nm in diameter) have been achieved with 515 nm laser beam in our previous paper [17]. There exists a shortest polymerization time for a single voxel to be polymerized above a monomer conversion threshold under a set of irradiation conditions (single pulse energy and repetition rate combinations). In low single pulse energy regime ($< 10 \mu J$), it is more energy-efficient to use fewer and higher-energy pulses within the same polymerization time. However, this trend reverses when the termination by R-R recombination becomes more severe in the regime of high single pulse energy (10 μJ -30 μ J), where over 90% of the generated radicals are wasted due to R-R recombination. Also, in the investigated regime, the local temperature increase during the entire polymerization time is negligibly small and is mainly attributed to the exothermic polymerization reaction. Although this paper focuses on the strong-pulse regime with repetition rates in the range of 1-100 kHz, it would be interesting to investigate "intermediate" repetition rates between 100 kHz and 100 MHz [39]. A transition is expected in this regime that could contain new processing conditions with advantages such as wide processing window, small linewidth, etc. Combined with the results reported in this paper, this will reveal new insights of how to improve the efficacy of photopolymerization for high-throughput and energy-efficient microfabrication.

Funding

This research was partially supported by NSF grants No. 1711356, 1846671, and 1712469.

CRediT authorship contribution statement

Mingman Sun: Writing – original draft, Writing – review & editing, Methodology, Software, Data curation, Visualization, Formal analysis, He Chang: Validation, Investigation, Formal analysis, Pooria Golvari:

Writing – original draft, Writing – review & editing, Investigation, Formal analysis, **Stephen M. Kuebler:** Conceptualization, Supervision, Funding acquisition, Writing – review & editing, **Xiaoming Yu:** Conceptualization, Supervision, Funding acquisition, Writing – review & editing, **Meng Zhang:** Conceptualization, Supervision, Funding acquisition, Writing – review & editing.

Declaration of Competing Interest

The authors declare that they have no known competing financial interests or personal relationships that could have appeared to influence the work reported in this paper.

Data availability

Data will be made available on request.

Acknowledgements

We thank Chun Xia for participating in helpful discussions of this work.

Appendix A. Supporting information

Supplementary data associated with this article can be found in the online version at doi:10.1016/j.addma.2022.103241.

References

- [1] T.D. Ngo, A. Kashani, G. Imbalzano, K.T.Q. Nguyen, D. Hui, Additive manufacturing (3D printing): a review of materials, methods, applications and challenges, Compos. Part B Eng. 143 (2018) 172–196.
- [2] X. Wang, M. Jiang, Z. Zhou, J. Gou, D. Hui, 3D printing of polymer matrix composites: a review and prospective, Compos. Part B Eng. 110 (2017) 442–458.
- [3] B.E. Kelly, I. Bhattacharya, H. Heidari, M. Shusteff, C.M. Spadaccini, H.K. Taylor, Volumetric additive manufacturing via tomographic reconstruction, Science 363 (2019) 1075–1079.
- [4] M. Regehly, Y. Garmshausen, M. Reuter, N.F. König, E. Israel, D.P. Kelly, C.-Y. Chou, K. Koch, B. Asfari, S. Hecht, Xolography for linear volumetric 3D printing, Nature 588 (2020) 620–624.
- [5] J.B. Mueller, J. Fischer, F. Mayer, M. Kadic, M. Wegener, Polymerization kinetics in three-dimensional direct laser writing, Adv. Mater. (2014) 6566–6571.
- [6] Q. Geng, D. Wang, P. Chen, S.-C. Chen, Ultrafast multi-focus 3-D nano-fabrication based on two-photon polymerization, Nat. Commun. 10 (2019) 2179.
- [7] S.K. Saha, D. Wang, V.H. Nguyen, Y. Chang, J.S. Oakdale, S.-C. Chen, Scalable submicrometer additive manufacturing, Science 366 (2019) 105–109.
- [8] J. Fischer, M. Wegener, Three-dimensional optical laser lithography beyond the diffraction limit, Laser Photonics Rev. 7 (2013) 22–44.
- [9] C.W. Hull, Apparatus for production of three-dimensional objects by stereolithography, US Pat. 4575330 (1986) 1–16.

- [10] Q. Mu, L. Wang, C.K. Dunn, X. Kuang, F. Duan, Z. Zhang, H.J. Qi, T. Wang, Digital light processing 3D printing of conductive complex structures, Addit. Manuf. 18 (2017) 74–83.
- [11] G. Odian. Principles of Polymerization, 4th ed..., Wiley,, 2004.
- [12] J. Stampfl, R. Liska, A. Ovsianikov. Multiphoton Lithography: Techniques, Materials, and Applications, 1st edition., Wiley-VCH., 2016.
- [13] M. Malinauskas, M. Farsari, A. Piskarskas, S. Juodkazis, Ultrafast laser nanostructuring of photopolymers: a decade of advances, Phys. Rep. 533 (2013) 1–31
- [14] A. Pikulin, N. Bityurin, Spatial resolution in polymerization of sample features at nanoscale, Phys. Rev. B 75 (2007), 195430.
- [15] L. Yang, A. Münchinger, M. Kadic, V. Hahn, F. Mayer, E. Blasco, C. Barner-Kowollik, M. Wegener, On the Schwarzschild Effect in 3D Two-Photon Laser Lithography, Adv. Opt. Mater. 7 (2019) 1901040.
- [16] M. Malinauskas, A. Žukauskas, G. Bičkauskaitė, R. Gadonas, S. Juodkazis, Mechanisms of three-dimensional structuring of photo-polymers by tightly focussed femtosecond laser pulses, Opt. Express 18 (2010) 10209.
- [17] H. Cheng, C. Xia, M. Zhang, S.M. Kuebler, X. Yu, Fabrication of high-aspect-ratio structures using Bessel-beam-activated photopolymerization, Appl. Opt. 58 (2019) 201
- [18] J.I. Kato, N. Takeyasu, Y. Adachi, Sun Hong-Bo, and S. Kawata, Multiple-spot parallel processing for laser micronanofabrication, Appl. Phys. Lett. 86 (2005) 1–4.
- [19] M. Watabe, K. Miyamoto, and T. Omatsu, Spiral relief formation in an azo-polymer film by the irradiation of a circularly polarized optical vortex beam, in 2013 Conference on Lasers & Electro-Optics Europe & International Quantum Electronics Conference CLEO EUROPE/IQEC (2013), pp. 1–1.
- [20] H. Cheng, P. Golvari, C. Xia, M. Sun, M. Zhang, S.M. Kuebler, X. Yu, High-throughput microfabrication of axially tunable helices, Photonics Res 10 (2022) 303
- [21] D. Mansour, D.G. Papazoglou, Tailoring the focal region of abruptly autofocusing and autodefocusing ring-Airy beams, OSA Contin. 1 (2018) 104–115.
- [22] H. Cheng, C. Xia, S.M. Kuebler, P. Golvari, M. Sun, M. Zhang, X. Yu, Generation of Bessel-beam arrays for parallel fabrication in two-photon polymerization, J. Laser Appl. 33 (2021), 012040.
- [23] S. Kawata, H.B. Sun, T. Tanaka, K. Takada, Finer features for functional microdevices, Nature 412 (2001) 697–698.
- [24] J.B. Mueller, J. Fischer, M. Wegener, Chapter 3.1 Reaction mechanisms and in situ process diagnostics (Micro and Nano Technologies), in: T. Baldacchini (Ed.), Three-Dimensional Microfabrication Using Two-Photon Polymerization, Second edition., William Andrew Publishing, 2020, pp. 175–196 (Micro and Nano Technologies).
- [25] J.B. Müller, Exploring the Mechanisms of Three-Dimensional Direct Laser Writing by Multi-Photon Polymerization, (https://publikationen.bibliothek.kit.edu/10000 47792).

- [26] J. Serbin, A. Egbert, A. Ostendorf, B.N. Chichkov, R. Houbertz, G. Domann, J. Schulz, C. Cronauer, L. Fröhlich, M. Popall, Femtosecond laser-induced twophoton polymerization of inorganic-organic hybrid materials for applications in photonics, Opt. Lett. 28 (2003) 301.
- [27] N. Uppal, Modeling of temperature-dependent diffusion and polymerization kinetics and their effects on two-photon polymerization dynamics, J. Micron MEMS MOEMS 7 (2008), 043002.
- [28] K.S. Anseth, C.M. Wang, C.N. Bowman, Reaction behaviour and kinetic constants for photopolymerizations of multi(meth)acrylate monomers, Polymer 35 (1994) 3243–3250.
- [29] M.S. Matheson, E.E. Auer, E.B. Bevilacqua, E.J. Hart, Rate constants in free radical polymerizations. i. methyl methacrylate, J. Am. Chem. Soc. 71 (1949) 497–504.
- [30] R. Wollhofen, B. Buchegger, C. Eder, J. Jacak, J. Kreutzer, T.A. Klar, Functional photoresists for sub-diffraction stimulated emission depletion lithography, Opt. Mater. Express 7 (2017) 2538–2559.
- [31] O. Soppera, S. Jradi, D.J. Lougnot, Photopolymerization with microscale resolution: influence of the physico-chemical and photonic parameters, J. Polym. Sci. Part Polym. Chem. 46 (2008) 3783–3794.
- [32] K.J. Schafer, J.M. Hales, M. Balu, K.D. Belfield, E.W. Van, Stryland, D.J. Hagan, Two-photon absorption cross-sections of common photoinitiators, J. Photochem. Photobiol. Chem. 162 (2004) 497–502.
- [33] T. Majima, W. Schnabel, On the reactivity of phosphinoyl and thiophosphinoyl radicals: Flash photolysis studies, J. Photochem. Photobiol. Chem. 50 (1989) 21, 20
- [34] Additive manufacture of complex 3D Au-containing nanocomposites by simultaneous two-photon polymerisation and photoreduction | Scientific Reports, (https://www.nature.com/articles/s41598-017-17391-1).
- [35] J. Segurola, N.S. Allen, M. Edge, A. McMahon, S. Wilson, Photoyellowing and discolouration of UV cured acrylated clear coatings systems: influence of photoinitiator type, Polym. Degrad. Stab. 64 (1999) 39–48.
- [36] S.K. Saha, C. Divin, J.A. Cuadra, R.M. Panas, Effect of proximity of features on the damage threshold during submicron additive manufacturing via two-photon polymerization, J. Micro Nano-Manuf. 5 (2017), 031002.
- [37] J.B. Mueller, J. Fischer, Y.J. Mange, T. Nann, M. Wegener, In-situ local temperature measurement during three-dimensional direct laser writing, Appl. Phys. Lett. 103 (2013) 0-4.
- [38] A.K. O'Brien, C.N. Bowman, Impact of oxygen on photopolymerization kinetics and polymer structure, Macromolecules 39 (2006) 2501–2506.
- [39] J. Fischer, J.B. Mueller, J. Kaschke, T.J. a Wolf, A.-N. Unterreiner, M. Wegener, Three-dimensional multi-photon direct laser writing with variable repetition rate, Opt. Express 21 (2013) 26244–26260.